TECHNOLOGIE 5G

Bulletin de veille scientifique : Mars 2025

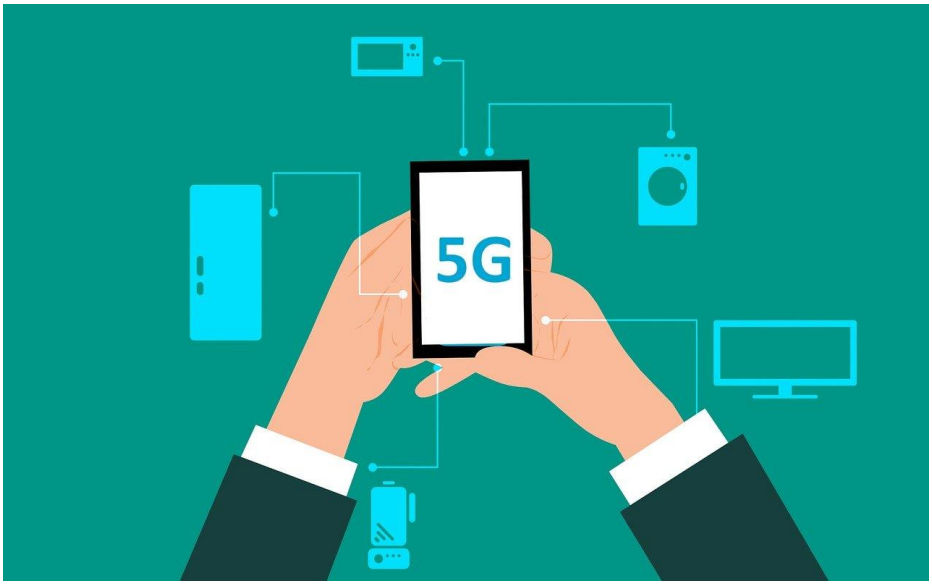

Objectifs : réaliser une veille scientifique sur la technologie 5G

La validation des informations fournies (exactitude, fiabilité, pertinence par rapport aux principes de prévention, etc.) est du ressort des auteurs des articles signalés dans la veille. Les informations ne sont pas le reflet de la position de l'INRS. Les éléments issus de cette veille sont founis sans garantie d'exhaustivité. Les liens mentionnés dans le bulletin donnent accès aux documents sous réserve d'un abonnement à la ressource.

Les bulletins de veille sont disponibles sur le portail documentaire de l'INRS. L'abonnement permet de recevoir une alerte mail lors de la publication d'un nouveau bulletin (bouton « M'abonner » disponible après connexion à son compte).

Généralités

Aucun article dans ce bulletin.

Performances et sécurité

A new approach to interference cancellation in D2D 5G uplink via Non orthogonal convex optimization.

Zhu M, Guo P, Liu X, Zhang H, Othmen S, Lhioui C, et al. *Sci Rep*. 2025 Mar 1;15(1):7253.

Heterogeneous communication modes in 5G demand integrated device connections, resource availability, and high capacity for meeting user demands. The radio resource allocation and usage for massive users results in interference between the device-to-device (D2D) uplink channels. This issue is addressed using a Non-orthogonal Convex Optimization Problem (NCOP) that identifies the chances of self-interference cancellations. This technique classifies interference and non-interference allocations in the rate of uplink communications. The channel reassignment is addressed as an NCOP based on the available interference levels. The interference levels before and after allocation and reallocation are analyzed under convex optimization. The interference cancellation convergence is computed for both channels wherein the transfer switching is performed. The convergence rate is estimated using the interference level and the number of channels reassigned for the uplink devices. Hence, the self-interference cancellation relies on non-convex channel allocations across various switching in this case. This feature is revisited if the D2D channels exceed their capacity for communication. Therefore, the 5G communication features coexist with the D2D uplinks for interference cancellations to improve channel allocation. For the SNR = 45dBm, the proposed NCOP reduces 12.4% of channel reassignment by augmenting 9.24% of interference cancellation.

Lien vers l'article

High-speed threat detection in 5G SDN with particle swarm optimizer integrated GRU-driven generative adversarial network.

Shameli R, Rajkumar S. *Sci Rep*. 2025 Mar 23;15(1):10025.

Detecting attacks in 5G software-defined network (SDN) environments requires a comprehensive approach that leverages traditional security measures, such as firewalls, intrusion prevention systems, and specialized techniques personalized to the unique characteristics of a 5G network. The attack detection in 5G SDN involves Machine learning (ML) and Deep learning (DL) algorithms to analyze large volumes of network data and identify patterns indicative of attacks. The study's main objective is to develop an efficient DL model to improve the detection performance and respond to security breaches effectively in a 5G SDN environment. The DL model integrates the Particle Swarm Optimizer-Gated Recurrent Unit Layer-Generative Adversarial Network-Intrusion Detection System classifier (PSO-GRUGAN-IDS). The PSO optimizes the network weight of the GAN model to improve the backpropagation while generating the synthetic data (attack data) in the generator model using GRU. The discriminator model uses the PSO-optimized generator model to produce synthetic and real attack data to forecast the attack. Finally, a deep classification (IDS) model is trained using a GRU network with a GAN model-produced attack data and real data to classify whether the SDN traffic is malicious or normal. Moreover, the performance of this model is evaluated using the InSDN dataset and compared with existing DL model-based intrusion detection approaches and the results demonstrate a significantly higher accuracy rate of 98.4%, precision rate of 98%, recall rate of 98.5%, less detection

time of 2.464 s, lesser Log loss rate of 1.0 and more metrics instilling confidence in the effectiveness of the proposed method.

Lien vers l'article

Resource allocation Of 5G mmWave communication under random interference.

Yuan L, Chen H, Huang Q, Gong J. *Sci Rep*. 2025 Mar 17;15(1):9120.

The swift expansion of artificial intelligence (AI) has revolutionized various sectors, driving innovation and efficiency across numerous industries. High-speed application scenarios and the fifth generation mobile communication systems (5G), the demand for communication resources is greater, and higher demand standards are put forward for future wireless communications, and the resource allocation problems of 5G communication systems also need to be further optimized. Key problems worth exploring in the study of communication technology include how to maximize the resource allocation efficiency of millimeter wave (mmWave), how to meet the developmental needs of communication technology and address user requirements, and how to minimize the system's total energy consumption. This paper constructs a mmWave system model, studies the mmWave channel model and the multi-beam model, proposes an optimal power algorithm to improve the resource allocation efficiency, simulates the proposed algorithm by MATLAB. The simulation results show that the direct path can enhance the coverage area's capacity.

Lien vers l'article

Optimizing power allocation for URLLC-D2D in 5G networks with Rician fading channel.

Muhammad O, Jiang H, Bilal M, Muhammad Umer M. *PeerJ Comput Sci*. 2025;11:e2712.

The rapid evolution of wireless technologies within the 5G network brings significant challenges in managing the increased connectivity and traffic of mobile devices. This enhanced connectivity brings challenges for base stations, which must handle increased traffic and efficiently serve a growing number of mobile devices. One of the key solutions to address these challenges is integrating device-to-device (D2D) communication with ultra-reliable and low-latency communication (URLLC). This study examines the impact of the Rician fading channel on the performance of D2D communication under URLLC. It addresses the critical problem of optimizing power allocation to maximize the minimum data rate in D2D communication. A significant challenge arises due to interference issues, as the problem of maximizing the minimum data rate is non-convex, which leads to high computational complexity. This complexity makes it difficult to derive optimal solutions efficiently. To address this challenge, we introduce an algorithm that is based on derivatives to find the optimal power allocation. Comparisons are made with the branch and bound (B&B) algorithm, heuristic algorithm, and particle swarm optimization (PSO) algorithm. Our proposed algorithm improves power allocation performance and also achieves faster execution with lower computational complexity compared to the B&B, PSO, and heuristic algorithms.

Lien vers l'article

Dielectric response mechanism and structure-property relationships of SrSn(BO(3))(2) microwave ceramics with ultra-low permittivity and their application for 5G microstrip patch antenna.

Yu Y, Wang X, An Z, Song F, Zhu W, Yao Z, et al. *Sci Rep*. 2025 Mar 18;15(1):9283.

In this work, strontium tin borate [SrSn(BO(3))(2), SSBO] microwave dielectric ceramics (MWDCs) were synthesized using the traditional solid-state sintering method at different sintering temperatures. The formation of phase-pure SSBO ceramics was determined by the Rietveld refinement of X-ray diffraction patterns, and the sample sintered at 1150 °C showed the densest micro-morphology. Lattice vibrational spectroscopy was used to interpret the intrinsic properties to develop structure-property relationships of the SSBO MWDCs. Seven distinct Raman-active vibrational modes were observed in the Raman spectra, and nine distinct vibrational modes were identified in the infrared spectra. The intrinsic dielectric properties were fitted and simulated by the four-parameter semi-quantum model according to the far-infrared reflection spectra of the ceramics. The dielectric responses of the SSBO ceramics were revealed based on their Raman and infrared spectra, and the microstructural origins of the dielectric responses were also clarified. Therefore, the correlations between the crystal structures and the dielectric properties of the SSBO ceramics were created from the Raman phonon modes. The B-O bond lengths and the A(g) mode shifts were closely related to the dielectric constants. The full-widths at half maximum of the ν(2) modes were positively correlated with the quality factor values. The SSBO ceramic sintered at 1150 °C exhibited the best dielectric properties of $\varepsilon(r) = 5.42$, $Q \times f = 32{,}618$ GHz ($f = 15.68$ GHz), and $\tau(f) = -48.28$ ppm/°C. This indicates that this sample was an ultra-low-permittivity MWDC with great potential for 5G applications. Simulation of this SSBO sample as a dielectric substrate was conducted using HFSS to fabricate a microstrip patch antenna capable of operating at 5.17 GHz, which exhibited a return loss (S11) of - 23.4 dB and a gain of 6.58 dBi.

Lien vers l'article

A Dual-Polarized and Broadband Multiple-Antenna System for 5G Cellular Communications.

Jahanbakhsh Basherlou H, Ojaroudi Parchin N, See CH. *Sensors (Basel)*. 2025 Feb 9;25(4).

This study presents a new multiple-input multiple-output (MIMO) antenna array system designed for sub-6 GHz fifth generation (5G) cellular applications. The design features eight compact trapezoid slot elements with L-shaped CPW (Coplanar Waveguide) feedlines, providing broad bandwidth and radiation/polarization diversity. The antenna elements are compact in size and function within the frequency spectrum spanning from 3.2 to 6 GHz. They have been strategically positioned at the peripheral corners of the smartphone mainboard, resulting in a compact overall footprint of 75 mm × 150 mm FR4. Within this design framework, there are four pairs of antennas, each aligned to offer both horizontal and vertical polarization options. In addition, despite the absence of decoupling structures, the adjacent elements in the array exhibit high isolation. The array demonstrates a good bandwidth of 2800 MHz, essential for 5G applications requiring high data rates and reliable connectivity, high radiation efficiency, and dual-polarized/full-coverage radiation. Furthermore, it achieves low ECC (Envelope Correlation Coefficient) and TARC (Total Active Reflection Coefficient) values, measuring better than 0.005 and -20 dB, respectively. With its compact and planar configuration, quite broad bandwidth, acceptable SAR (Specific Absorption Rate) and excellent radiation characteristics, this suggested MIMO antenna array design shows good promise for integration into 5G hand-portable devices. Furthermore, a compact phased-array millimeter-wave (mmWave) antenna with broad bandwidth is introduced as a proof of concept for higher frequency

antenna integration. This design underscores the potential to support future 5G and 6G applications, enabling advanced connectivity in smartphones.

Lien vers l'article

Machine learning enabled dual to wideband frequency agile [Formula: see text]ceramic-based dielectric MIMO antenna for 5G new radio applications.

Rai JK, Dwivedi AK, Singh V, Ranjan P, Sharma A, Pandey A. *Sci Rep*. 2025 Mar 20;15(1):9648.

This article presents a dual-band to wideband Frequency Agile (FA) rectangular dielectric resonator (DR) based hybrid MIMO antenna for 5G New Radio (NR) application with connected ground. The DR is made of Al(2)O(3) (ε(r) = 9.8) ceramic material. The FA is achieved through the PIN Diode switches. When the PIN Diode is in an "ON" state, it provides dual bands due to the excitation of TE(111) mode. When the PIN Diode is in an "OFF" state, it provides wideband characteristics due to the excitation of TE(111) and TE(211) modes in the rectangular DR. The isolation and gain are achieved by 20 dB and 4.3 dBi, respectively. The maximum tuning range is 49.36. The MIMO performance characteristics are achieved within the allowable range. A good agreement is achieved between the simulated and measured results. The suggested MIMO antenna is optimized through the various ML algorithms in which Random Forest (RF) ML algorithms achieved the highest accuracy more than 99% compared to other ML algorithms for S-parameters prediction. Hence, it is suitable for 5G NR applications.

Lien vers l'article

Antenna Design and Optimization for 5G, 6G, and IoT.

Jahanbakhsh Basherlou H, Ojaroudi Parchin N, See CH. *Sensors (Basel)*. 2025 Feb 28;25(5).

This Special Issue focuses on the latest advancements in antenna design and optimization for 5G, 6G, and IoT applications. The contributions presented in this collection explore cutting-edge methodologies, novel architecture, and emerging trends that are shaping the future of wireless communication. Topics range from innovative MIMO and phased-array configurations to the development of highly efficient THz and mmWave antennas, as well as AI-driven optimization techniques. By providing a comprehensive overview of state-of-the-art research, this Special Issue aims to foster new insights and inspire further exploration into next-generation antenna technologies. The research featured here not only highlights significant theoretical and experimental advancements but also underscores the transformative potential of antennas in shaping the future of connectivity.

Lien vers l'article

A compact single layer dual band microstrip patch antenna for 5G terminal applications.

Ding XH, Tan Z, Burokur SN. *Sci Rep*. 2025 Mar 12;15(1):8601.

In modern applications, the shrinking available space on terminals coupled with the increasing number of frequency bands has prompted the greatest demand for antenna miniaturization and multi-band features. This work introduces an innovative method for designing a dual-band planar antenna with an exceptionally compact size, addressing the pressing requirement. Two half-mode patches, both operating in two modes (TM(0.5,0) of 3.5 GHz frequency band and TM(0.5,2) of 4.9 GHz frequency

band) are placed back-to-back. The dual-mode operation in the 3.5 GHz band is achieved using the two TM(0.5,0) modes and the dual-mode operation in the 4.9 GHz band is obtained from the TM(0.5,2) and strip modes. Then, based on the elementary antenna design, a 4 × 4 MIMO system is designed and measured. The isolation between the elements is found to be greater than 15.5 dB. The proposed antenna achieves a bandwidth coverage of 3.36-3.70 GHz and 4.79-5.01 GHz, corresponding to N78 and N79 frequency bands of the fifth generation (5G) wireless communication systems, respectively. The proposed antenna, based on a single-layer design without any air spacing, features a compact size and high integration density, making it an interesting solution for 5G terminals.

Lien vers l'article

Metasurface-Loaded Biodegradable Mobile Phone Back Cover for Enhanced Radiation Performance.

Acharjee J, Ali J, Uzair M, Phakaew T, Akkaraekthalin P, Maiket Y, et al. *Materials (Basel)*. 2025 Feb 7;18(4).

This article introduces a novel biodegradable metasurface-loaded mobile phone back cover designed to reduce electromagnetic exposure and enhance antenna performance. The cover operates across the low GHz band (2-8 GHz) and the millimeter-wave band (22-25.6 GHz), utilizing polylactic acid as an eco-friendly substrate. Integrated with a six-port multiple-input multiple-output (MIMO) antenna system, the cover achieves port isolation above 20 dB in both bands. Specific absorption rate (SAR) analysis, performed using a human head model, shows significant reductions in electromagnetic exposure-61.1% in the low GHz band (from 1.06 W/kg to 0.412 W/kg) and 55% in the millimeter wave band (from 2.061 W/kg to 0.917 W/kg). Additionally, the metasurface cover enhances antenna gain and increases impedance bandwidth by 20% in the low GHz band and 8.3% in the millimeter-wave band. A comparative study highlights superior SAR reduction and bandwidth improvement of a metasurface on a biodegradable substrate over one on a silicone substrate. Prototypes of the MIMO antenna and the proposed cover were fabricated and tested, revealing strong alignment between simulated and measured results. These findings highlight the potential of biodegradable metasurface-based covers to deliver high-performance, sustainable solutions for mobile communication devices.

Lien vers l'article

High-Performance Series-Fed Array Multiple-Input Multiple-Output Antenna for Millimeter-Wave 5G Networks.

Alsaab N, Alhassoon K, Alsaleem F, Alsunaydih FN, Madbouly SO, Khaleel SA, et al. *Sensors (Basel)*. 2025 Feb 9;25(4).

This research presents a high-performance design for a multiple-input multiple-output (MIMO) antenna intended for operation within the 28 GHz band. The four-port MIMO antenna configuration, featuring 1 × 8 series-fed arrays for each port, has demonstrated peak gains of 15.5 dBi and bandwidths of 2 GHz. This improved antenna performance results from carefully optimized antenna spacing and a decoupling approach involving well-designed metamaterial cells, effectively minimizing interference between antenna elements. The system exhibits remarkably low mutual coupling, measuring below -40 dB, with envelope correlation coefficients of 0.00010, diversity gains nearing 10 dB, and a channel loss capacity of 0.11 bit/s/Hz across the frequency spectrum under investigation. Experimental evaluations have confirmed these improvements, establishing the proposed design as a robust candidate suitable for a wide range of millimeter-wave communication systems.
Lien vers l'article

Architecture réseau

NOMA-MIMO in 5G network: a detailed survey on enhancing data rate.

Halabouni M, Roslee M, Mitani S, Abuajwa O, Osman A, Binti Ali FZ, et al. *PeerJ Comput Sci*. 2025;11:e2388.

Non-orthogonal multiple access (NOMA) is a technology that leverages user channel gains, offers higher spectral efficiency, improves user fairness, better cell-edge throughput, increased reliability, and low latency, making it a potential technology for the next generation of cellular networks. The application of NOMA in the power domain (NOMA-PD) with multiple-input multiple-output (MIMO) and other emerging technologies allows to achieve the demand for higher data rates in next-generation networks. This survey aims to funnel down NOMA MIMO resource allocation issues and different optimization problems that exist in the literature to enhance the data rate. We examine the most recent NOMA-MIMO clustering, power allocation, and joint allocation schemes and analyze various parameters used in optimization methods to design 5G systems. We finally identify a promising research problem based on the signal-to-interference-plus-noise ratio (SINR) parameter in the context of NOMA-PD with MIMO configuration.

Lien vers l'article

Efficacité énergétique

Aucun article dans ce bulletin.

Autres équipements

Aucun article dans ce bulletin.

Applications médicales et industrielles de la 5G

Applications industrielles

Aucun article dans ce bulletin.

Applications médicales

A 5G network based conceptual framework for real-time malaria parasite detection from thick and thin blood smear slides using modified YOLOv5 model.

Lipsa S, Kumar Dash R, Cengiz K, Ivković N, Akhunzada A. *Digit Health*. 2025 Jan-Dec;11:20552076251321540.

OBJECTIVE: This paper aims to address the need for real-time malaria disease detection that integrates a faster prediction model with a robust underlying network. The study first proposes a 5G network-based healthcare system and then develops an automated malaria detection model capable of providing an accurate diagnosis, particularly in areas with limited diagnostic resources. METHODS: The proposed system leverages a deep learning-based YOLOv5x algorithm to detect malaria parasites in thick and thin blood smear samples. The YOLOv5x network architecture was modified by introducing two squeeze-and-excitation network (SENet) layers just before the Upsample layers. The system is designed to operate over 5G networks efficiently, enabling remote and smart healthcare solutions. RESULTS: The modified YOLOv5x model demonstrated improved accuracy and precision in detecting malaria parasites on microscopic slides. The inclusion of SENet layers optimized the network's performance, making it suitable for real-time disease detection over a 5G network. CONCLUSION: Our model exemplifies how a generic one-stage object detection algorithm, such as YOLOv5x, can be repurposed to detect objects as small as malaria parasites from microscopic visuals in a cost-effective manner over the 5G network. By integrating the computational efficiency of deep learning with the connectivity of 5G networks, this system can significantly enhance remote diagnostic capabilities and contribute to smart healthcare solutions.

Lien vers l'article

Secure and intelligent 5G-enabled remote patient monitoring using ANN and Choquet integral fuzzy VIKOR.

Chinnaperumal S, Periyasamy M, Alhussan AA, Kannan S, Khafaga DS, Raju SK, et al. *Sci Rep*. 2025 Mar 22;15(1):9913.

Rapid advancements in healthcare technologies necessitate efficient and secure remote patient monitoring systems. This research develops an intelligent system that combines ANN technology and 5G infrastructure with MCDM methods based on Choquet Integral Fuzzy VIKOR to improve medical data acquisition processes. Physical Layer Security (PLS) is a main emphasis point since it protects transmitted healthcare data from eavesdroppers and cyber intruders. The proposed model implements Reinforcement Learning with Hyper-parameter tuning and Lasso regression to obtain a 97.25% accuracy level, which exceeds Physical-Layer Authentication with Superimposed Independent

authentication Tags PLA-SIT (97%), Flexible Physical Layer Authentication FPLA (96.8%) and Privacy-Embedded Lightweight and Efficient Automated PLA (95.3%). The proposed model surpasses both CNN-based mechanisms by 94.7%, Shamir's Secret Sharing Algorithm by 90.7%, and the Blowfish Algorithm by 82.3%. The enhanced quality of service alongside reliability produces the model as a dependable solution for MIoT applications that will exist in the next generation.

Lien vers l'article

Evaluation (Mesure des niveaux d'exposition)

Méthodes d'évaluation

Aucun article dans ce bulletin.

Evaluation population générale

Auto-induced uplink 4G and 5G RF-EMF exposure assessment using a network monitoring application in different microenvironments across seven European countries.

Stroobandt B, Van Bladel H, Veludo AF, Deprez K, Aerts S, Verloock L, et al. *Environ Res*. 2025 Apr 1;270:121029.

The auto-induced uplink (a-UL) radio-frequency electromagnetic field (RF-EMF) exposure, often the dominant part of the total RF-EMF exposure, has not been included in previous microenvironmental studies. As 5G exposure depends more on mobile phone usage, monitoring typical transmit power levels is crucial towards more accurate personal exposure assessment. This study describes spatial differences in average mobile phone transmit power and investigates the influence of uplink duty cycles and frequency band usage. A novel methodology using the network monitoring application QualiPoc in fourth-generation (4G) and non-standalone fifth-generation (5G) networks was presented. For the first time, the assessment of 4G and 5G a-UL RF-EMF exposure was conducted simultaneously in a large-scale microenvironmental study in Europe. Measurements were performed along predefined routes in 282 different microenvironments (e.g., parks, residential areas) across seven European countries, during a maximum uplink usage scenario. The Netherlands had the highest average transmit powers per microenvironment (median 20.6 dBm). Transmit powers in villages were 0.6-2.1 dB higher than in big cities. The study suggested that base station density is a key predictor of a-UL exposure. Comparing technologies and frequency bands, average transmit powers for 5G were about 3.3 dB lower than for 4G and lowest for frequency bands with a time division duplexing (TDD) scheme due to the low uplink duty cycle (below 20%). This study provides crucial measurement data for epidemiologists and governments to enhance the understanding of the a-UL component of personal RF-EMF exposure.

Lien vers l'article

RF-EMF electromagnetic environment IN the West Bank, Palestine.

Lahham A, Alkhatib M. *Radiat Prot Dosimetry*. 2025 Mar 21;201(4):255-60.

With the increase in the distribution of sources of electromagnetic fields in the environment, public exposure to non-ionizing radiation emitted from these sources will increase and change with time. This work aims at the evaluation of public exposure to radiofrequency electromagnetic fields in the West Bank and compares this exposure with previous studies with a time interval difference of 11 years. Measurements of exposure were conducted in the outdoor environment in 149 locations using tri-axial E-field frequency-selective personal exposure meter EME SPY 140 enabling measurements of electric field strength in 14 predefined frequency bands in the range from 80 to 6 GHz. The average

field strength from all sources in all investigated locations was 1.4 Vm-1. The maximum exposure measured at any location in the country was 7.43 Vm-1 and was found in Ramallah City center. The exposure quotient corresponding to this value was about 19 times below unity. The total exposure quotient for all locations was 0.001 with FM broadcasting being the main contributor by about 36%, UMTS2100 downlink by 24%, GSM 900 downlink contributing by 17%, WiFi 5GHz by 9% GSM 1800 downlink by 5%. Seven other RF sources contributed together by only 9% including WiMax, TV, WiFi 2 GHz, and others. More than 90% of the electric field strength values were below the level of 3 Vm-1. Within 11 years the average total exposure coefficient increased by a factor of about 2.

Lien vers l'article

RF-EMF exposure assessment with add-on uplink exposure sensor in different microenvironments in seven European countries.

Bladel HV, Stroobandt B, Veludo AF, Deprez K, Röösli M, Tognola G, et al. *Environ Int*. 2025 Mar;197:109368.

INTRODUCTION: Several devices have been developed to assess exposure to radiofrequency electromagnetic field (RF-EMF). Since the existing solutions to measure the personal exposure induced by emerging 5G New Radio (NR) are expensive, complex, and bulky, a new cost efficient and low-complexity sensor is developed, that aims to measure RF-EMF exposure in different scenarios of data transmission within different areas. METHODS: With this novel sensor, activity-based microenvironmental surveys were conducted across seven European countries: Belgium, Hungary, Italy, Poland, Switzerland, the Netherlands, and the United Kingdom. The device is attached to a smartphone to quantify the auto-induced uplink (a-UL) transmission component of the total exposure for a broadband frequency range from 100 MHz to 6000 MHz and is thus denoted as add-on sensor. In-situ measurements were performed for three usage scenarios, namely non-user (i.e., environmental exposure), maximum downlink (max DL), and maximum uplink (max UL) scenarios, in a large city, a secondary city, and three rural villages a priori selected within each country. RESULTS: Power levels were lowest in non-user scenarios (median: -2.64 dBm or 0.54mW), increasing by a factor of 5.00 dB in maximum downlink scenarios and by a factor of 14.15 dB in maximum uplink scenarios. In the maximum uplink scenarios, the highest median a-UL power of 18.68dBm (= 73.79 mW) was recorded in The Netherlands, while the lowest median a-UL power of 4.77dBm (= 3 mW) was observed in the UK. The analysis of the measured data showed a prominent trend of a 2.72 dB lower power in the cities compared to the villages. Further comparisons were made based on microenvironment groups, where the lowest a-UL power levels (median: 12.35dBm) were measured in outdoor areas, with an increase of 1.78 dB and 1.91 dB in power was measured compared to public transport and public places, respectively. CONCLUSION: This study compares RF-EMF power levels between different countries, urbanization settings, and usage scenarios, which is important for future epidemiological studies.

Lien vers l'article

Risques professionnels

Aucun article dans ce bulletin.

Effets biologiques et sur la santé

In silico

Aucun article dans ce bulletin.

In vitro

Short-Term In Vitro Exposure of Human Blood to 5G Network Frequencies: Do Sex and Frequency Additionally Affect Erythrocyte Morphometry?

Žura N, Vince S, Perić P, Vilić M, Malarić K, Rimac V, et al. *Biomedicines*. 2025 Feb 15;13(2).

Background/Objectives: This study assessed the effects of 5G radiofrequency electromagnetic radiation (RF-EMR) at different frequencies (700 MHz, 2500 MHz, 3500 MHz) on the complete blood count (CBC), erythrocyte morphometry, and platelet activation after the short-term in vitro exposure of human blood. Methods: Blood samples from 30 healthy volunteers (15 men and 15 women, aged 25-40 years old) were collected at three intervals (14 days apart). For each collection, four tubes of blood were drawn per volunteer-two experimental and two controls. Experimental samples were exposed to 5G RF-EMR for 2 h at room temperature using a half-cone gigahertz transverse electromagnetic cell. The CBC was analysed via a haematology analyser, the erythrocyte morphometry was analysed using the SFORM program, and platelet activation was analysed via flow cytometry. Results: The CBC and platelet activation showed no significant differences between the experimental and control samples. However, the erythrocyte morphometry exhibited notable changes. At 700 MHz, the erythrocyte size, contour, and membrane roughness increased significantly for both sexes, with women's cells showing greater sensitivity. At 2500 MHz, women exhibited an increased contour index and a decreased solidity and form factor. At 3500 MHz, women showed an increased contour index and outline but a decreased solidity, elongation, and form factor. Cluster analysis identified two erythrocyte subpopulations: smaller, rounder cells with smooth membranes and larger cells with rougher membranes. Conclusions: These results indicate that 5G RF-EMR exposure significantly alters erythrocyte morphometry. The strongest effects were observed at 700 MHz, where men exhibited greater membrane roughness, and women showed larger and rounder erythrocytes. These findings suggest that short-term in vitro 5G RF-EMR exposure disrupts the cytoskeleton, increasing membrane permeability and deformability.

Lien vers l'article

Mechanistic insights into microwave radiation induced cognitive impairments: The role of m(6)A epigenetic modifications and HNRNPA2B1 in TrkB regulation.

Zhi W, Tang J, Zhang M, Zou Y, Qiao S, Ma L, et al. *Ecotoxicol Environ Saf*. 2025 Mar 1;292:117907.

Microwave radiation, a prevalent environmental stressor, significantly impacts human health. Based on previous studies, we hypothesize that microwave-induced cognitive impairments and vulnerability in the hippocampal dentate gyrus (DG) region are due to abnormal synaptic plasticity regulated by both newborn and mature neurons derived from neural stem cells (NSCs). Epigenetics links external factors to organisms, offers insights into the health effects of environmental influences. To explore the molecular mechanisms underlying the effects of microwave radiation on neuronal synaptic plasticity from the perspective of mRNA N(6)-methyladenosine (m(6)A) modification. We first assessed the impact of microwave radiation on cognitive memory abilities in rats through behavioral tests. Immunofluorescence staining were applied to clarify the influence of microwave radiation on both neurons and NSCs. Molecular mechanisms were investigated by ELISA, q-PCR, Western blot, MeRIP-seq, and RNA pull-down experiments. The microwave radiated rat model exhibiting learning and memory deficits. Impaired synaptic plasticity in mature hippocampal neurons alongside hindered NSCs proliferation and development were observed. Using our established non-contact co-culture model, we replicated the in vivo adverse effects of microwave radiation. Down-regulated HNRNPA2B1 leads to reduced binding of TrkB m(6)A and promoted TrkB degradation. This feedback loop results in low BDNF expression, ultimately causing cognitive impairments. Our study emphasizes the neurotoxicity of microwave radiation and identifies TrkB m(6)A modification as a potential target for protecting against cognitive damage induced by electromagnetic radiation.

Lien vers l'article

Protective Effects and Mechanisms of Astragaloside on Microwave Radiation-induced Cardiac Injury.

Zhang X, Zhao L, Hu S, Miao C, Dong J, Zhang J, et al. *Radiat Res*. 2025 Mar 1;203(3):142-54.

This study explores the potential protective effects and mechanisms of astragaloside (AST) on microwave radiation-induced cardiac injury. Rats and H9c2 cells were irradiated with S-band microwave to induce in vivo and in vitro cardiac injury models. In irradiated rats, experiments such as electrophysiological examination, serum biochemical analysis, hematoxylin and eosin (H&E) staining, transmission electron microscopy (TEM), western blot, and immunohistochemical staining were performed after AST were administrated for 7 and/or 14 days. In irradiated H9c2 cells that were pretreated with 1-Azakenpaullone (glycogen synthase kinase-3β inhibitor) or AST, experiments such as TEM, cell counting kit-8 assay, western blot, tetramethylrhodamine methylester staining, and determination of reactive oxygen species (ROS), adenosine triphosphate (ATP) and mitochondrial membrane potential (MMP) were performed. In vivo results showed that at 7 days after exposure, microwave radiation-induced severe cardiac injury (as evidenced by abnormal electrocardiograms and cardiac tissue structure, increased serum myocardial enzyme activities and Ca2+ concentration) and lower level of phosphorylation of glycogen synthase kinase-3β (p-GSK-3βSer9). All these changes were reversed after AST treatment. The results of in vitro experiments showed that microwave radiation induced a lower level of p-GSK-3βSer9, more mitochondrial permeability transition pore (mPTP) opening and more serious mitochondrial dysfunction (characterized by increased intracellular ROS production, decreased intracellular ATP synthesis and MMP decline) in H9c2 cells. All these changes were reversed by 1-Azakenpaullone and AST pretreatment. The findings suggest that AST could shield

against microwave radiation-induced cardiac injury by promoting the phosphorylation of GSK-3βSer9, thereby inhibiting mPTP opening and restoring mitochondrial function. This study offers valuable insights into potential therapeutic strategies for mitigating the adverse effects of microwave radiation on cardiac health.

Lien vers l'article

Effects of 1800 MHz and 2100 MHz mobile phone radiation on the blood-brain barrier of New Zealand rabbits.

Kizilçay AO, Tütüncü B, Koçarslan M, Gözel MA. *Med Biol Eng Comput*. 2025 Mar;63(3):915-32.

In this study, the impact of mobile phone radiation on blood-brain barrier (BBB) permeability was investigated. A total of 21 New Zealand rabbits were used for the experiments, divided into three groups, each consisting of 7 rabbits. One group served as the control, while the other two were exposed to electromagnetic radiation at frequencies of 1800 MHz with a distance of 14.5 cm and 2100 MHz with a distance of 17 cm, maintaining a constant power intensity of 15 dBm, for a duration equivalent to the current average daily conversation time of 38 min. The exposure was conducted under non-thermal conditions, with RF radiation levels approximately ten times lower than normal values. Evans blue (EB) dye was used as a marker to assess BBB permeability. EB binds to plasma proteins, and its presence in brain tissue indicates a disruption in BBB integrity, allowing for a quantitative evaluation of radiation-induced permeability changes. Left and right brain tissue samples were analyzed using trichloroacetic acid (TCA) and phosphate-buffered solution (PBS) solutions to measure EB amounts at 620 nm via spectrophotometry. After the experiments, BBB tissue samples were collected from the right and left brains of all rabbits in the three groups and subjected to a series of medical procedures. Samples from Group 1 were compared with those from Group 2 and Group 3 using statistical methods to determine if there were any significant differences. As a result, it was found that there was no statistically significant difference in the BBB of rabbits exposed to 1800 MHz radiation, whereas there was a statistically significant difference at a 95% confidence level in the BBB of rabbits exposed to 2100 MHz radiation. A decrease in EB values was observed upon the arithmetic examination of the BBB.

Lien vers l'article

Sur l'homme

Brain Disease-Modifying Effects of Radiofrequency as a Non-Contact Neuronal Stimulation Technology.

Sun S, Bok J, Jang Y, Seo H. *Int J Mol Sci*. 2025 Mar 4;26(5).

Non-invasive, non-contact, and painless methods of electrical stimulation to enhance neural function have been widely studied in recent years, particularly in the context of neurodegenerative diseases such as Alzheimer's disease (AD) and related dementias, which cause cognitive decline and other neurological symptoms. Radiofrequency (RF), which is a rate of oscillation in the range of 3 kHz to 300 GHz (3 THz), has been suggested as one potential non-contact neuronal stimulation (NCNS) technique for improving brain function. A new type of electrical stimulation uses a radiofrequency electromagnetic field (RF-EMF). RF exposure has been shown to modulate neural stimulation and influence various brain activities in in vitro and in vivo models. Recent studies have explored the effects

of RF-EMF on human physiology, particularly in areas such as brain activity, cognition, and sleep behavior. In this review, we summarize recent findings about the effects of non-contact stimulations in in vitro studies, in vivo animal models, and human clinical cases.

Lien vers l'article

Reproduction

Transcriptomic and metabolic profiling reveals the effects of long-term microwave exposure on testicular tissue.

Yao B, Zeng J, Shi J, Pang Y, Men J, Li Y, et al. *Ecotoxicol Environ Saf*. 2025 Mar 15;293:118040.

The effect of electromagnetic exposure on health is becoming increasingly important as it affects many aspects of human life and health. However, the effects in environmental electromagnetic fields on the male reproductive system were still controversial, and the impacts of long-term microwave exposure on testicular tissue remain poorly defined. This study exposed rats to 30 mW/cm(2) of microwave radiation (2.856 GHz) for six weeks and revealed that long-term microwave exposure damaged the testis structures, sperm motility, and morphology, affected hormone levels, energy metabolism, and induced oxidative stress. Assays for bulk RNA, metabonomics, single-cell RNA, and transposase-accessible chromatin with high-throughput sequencing were performed to analyze the transcriptional and metabolic atlas of testicular damage after microwave radiation. Differentially expressed genes were enriched in oxidative stress and energy metabolism pathways. Furthermore, ten subgroups were identified with scRNA-seq, including five developmental phases of germ cells, and radiation-associated changes in cell composition, especially stuck in round spermatids, were observed. Radiation significantly upregulated the expression of Atp6v1e2 in round spermatids and enriched the expression of many transcription factors by disturbing the accessibility profile of chromatin. This study provides effective insights into the long-term impacts of microwave radiation on male reproduction.

Lien vers l'article

Oxidative stress and energy metabolism in male reproductive damage from single and combined high-power microwave exposure at 1.5 and 4.3GHz.

Li Y, Yao B, Men J, Pang Y, Gao J, Bai Y, et al. *Reprod Toxicol*. 2025 Mar;132:108759.

The effect of multi-frequency electromagnetic environments on male reproduction has attracted the medical community's interest. Studies have investigated the effects and mechanisms of single-frequency microwave exposure on male reproduction, but comparative research on high-power microwave (HPM) composite and single exposure remains scarce. This study aimed to examine the effects and mechanisms of combined 1.5 GHz and 4.3 GHz microwave exposure on male reproduction. Male Wistar rats were exposed to 1.5 GHz (L-band) and 4.3 GHz (C-band) electromagnetic radiation for 15 minutes. The four groups were: sham, 10 mW/cm² L-band, 10 mW/cm² C-band, and 5 mW/cm² L-band and 5 mW/cm² C-band compound. Assessments were made on the pathological structures of testes, sperm viability, serum sex hormones, oxidative stress, and energy metabolism levels after radiation. Exposure to 1.5 GHz and 4.3 GHz microwaves individually resulted in testicular tissue damage and reduced sperm quality. There was little difference between the damage caused by HPM composite and single exposure. The exposed groups showed histological and ultrastructural changes, with reduced spermatozoa viability, motility parameters, and serum testosterone, luteinizing hormone, follicle-stimulating hormone, and serum inhibin-B on days 1 and 7 after exposure. These tended to recover partially by day 14. Adenosine triphosphate content and lactate dehydrogenase and succinate dehydrogenase activities in the exposed testicular tissue decreased, corresponding to decreased superoxide dismutase activity and increased malondialdehyde content. Both single and combined exposure to L- and C-band HPM affect the male reproductive system. Exposure to single and compound HPM shows no significant difference in risks, with oxidative stress and energy metabolism disturbances playing key roles.

Lien vers l'article

Dispositifs médicaux implantables

Aucun article dans ce bulletin.